Supplementary Figures

Historic creep events on Calaveras Fault

The USGS installed 4 creepmeters on the Calaveras Fault (Figure 1.1). Creepmeter XSH1 operated from 1971 to 1997 with 1-day sampling and was reactivated in October 2020 with 10-minute sampling. The other three creepmeters, SHR2, HLC1, and HLD1, were manually monitored from 1970 to 1999 but are currently not in operation. Data recorded by these instruments are plotted as Figure S1. XSH1 recorded at least 6 creep events with slip larger than 10 mm (Figure S1. A-F). Any creep events between 1988 and 2000 are not plotted here because of problems with the instrument or data.

Fig.S1. Historic creep events recorded by creepmeters XSH1, HLC1, and HLD1.

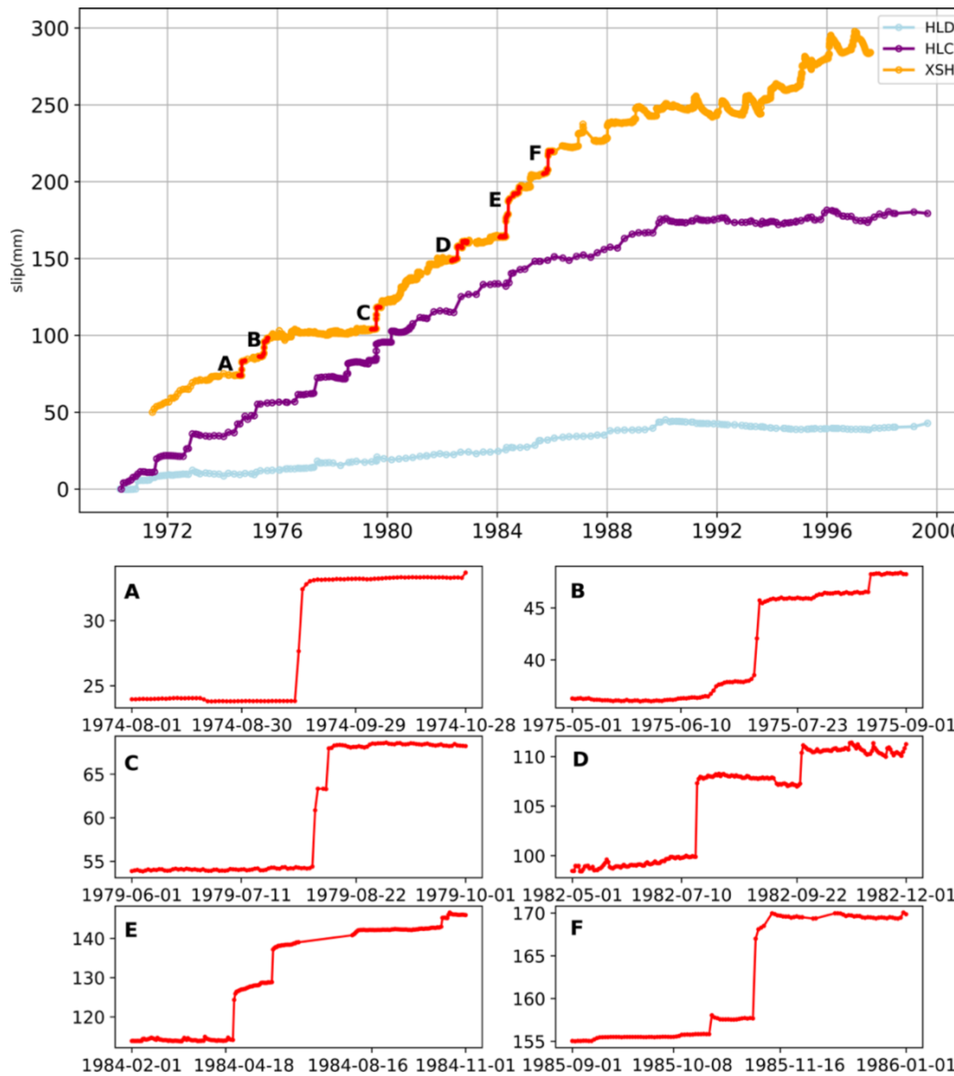

Uncertainty in earthquake location and magnitude

To obtain a better understanding of the spatiotemporal patterns of seismic activity during the 2021 creep event on the Calaveras fault, we improved the location quality of the catalog. We did a visual inspection of the arrivals picked by PhaseNet and EQCorrscan (Chamberlain et al., 2018; Zhu & Beroza, 2018), and we conducted a careful examination of all the seismic waveforms from selected stations in 2021 to prevent missed picks. We used the Hypoinverse location algorithm, and applied the station corrections and multiple 1-D velocity models used by the NCEDC in their catalog creation to alleviate the impact of local topography and instrument effects (Oppenheimer et al., 1993). We compared our locations with those from the NCEDC catalog for the same earthquakes and find that the differences are acceptable (Figure S2). Despite the absence of station correction files for 5 stations and the limitation of seismic station coverage, the Root-Mean-Square (RMS) traveltime residuals for 90% of the earthquake locations are lower than 0.35 seconds (Figure S3). Since we use fewer arrival information and stations, it is reasonable that we get higher RMS than the NCEDC catalog. The GrowClust relocation step incorporates earthquakes from 2012 to 2020 to minimize the differential arrival times (Trugman & Shearer, 2017). A higher cross-correlation threshold mitigates the RMS error of differential travel times while decreasing the number of clustered and relocated earthquakes. We tested various cross-correlation threshold (Table S1 and S2). And we set the cross-correlation threshold as 0.9, and the RMS differential travel times of 95% relocated events are lower than 0.1s (Table S1). Consequently, all earthquake locations are satisfactory, and the location of the relocated earthquakes is more accurate than the earthquakes that are not relocated.

Fig.S2. Comparison of our locations and those from the NCEDC catalog for the same earthquakes in 2021

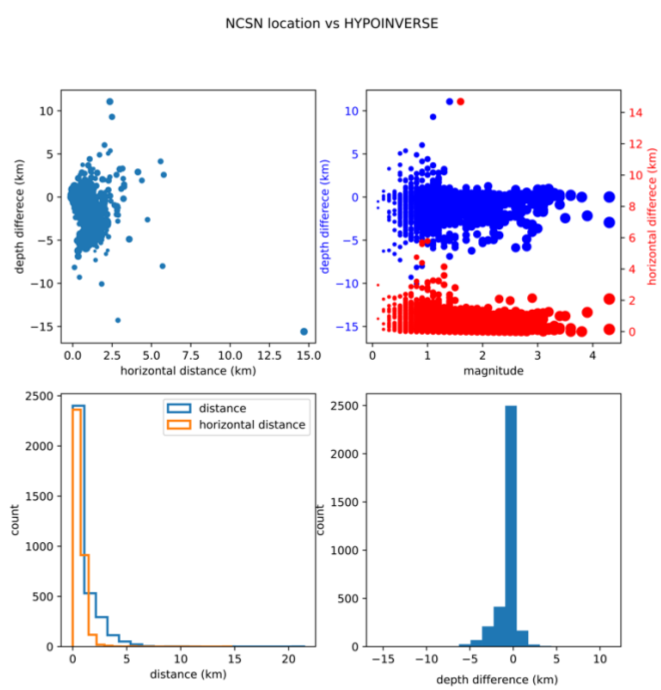

Fig.S3. Distribution of RMS travel time residuals for Hypoinverse locations. The left panel is for our catalog. The right panel is for the NCEDC catalog.

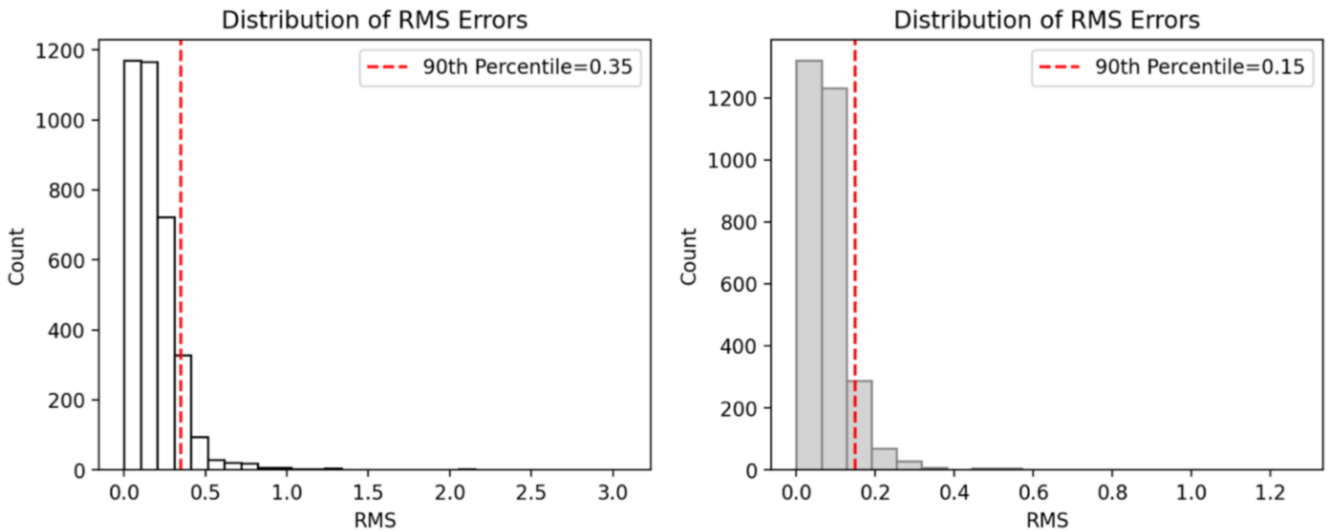

Table.S1. Table of GrowClust location differential traveltimes using different Cross-Correlation threshold

Cross-correlation coefficient threshold	pRMS mean	pRMS 95th percentile	sRMS mean	sRMS 95th percentile
0.4	0.096	0.2	0.15	0.41
0.5	0.08	0.18	0.111	0.28
0.6	0.079	0.19	0.097	0.27
0.8	0.058	0.17	0.043	0.15
0.9	0.03	0.1	0.026	0.11

Table.S2. Table of GrowClust clustered rate using different Cross-Correlation threshold

Cross-correlation coefficient threshold	Clustered rate
0.4	82.33%
0.5	82.15%
0.6	81.78%
0.8	75.38%
0.9	60.97%

Earthquakes above magnitude completeness

To show that the seismicity gap is not an artifact caused by heterogenous completeness, we plotted Figure 4 and Figure 5 with the earthquakes above magnitude completeness 0.5 here. Historical events were also selected according to a magnitude completeness threshold of 1.4. As shown in Figure S4 and Figure S5, the seismicity gap around latitude 36.91 is consistent with the selected events exceeding magnitude completeness.

Figure S4. Distribution and Characteristics of Detected Earthquakes above magnitude completeness (March-August 2021). (a) Map view and (b) cross-sectional profile illustrating the spatial distribution of detected earthquakes, symbolized by circles and squares (newly detected). All detected earthquakes are selected within 1km on the left side and 3km on the right side to the Calaveras fault, and they are sized by local magnitude and colored by occurrence time. Circles with black edges indicate earthquakes that were clustered and relocated by GrowClust, circles with gray edges are earthquakes not clustered. Gray dots are earthquakes above magnitude completeness included in the NCEDC catalog from 2012 to 2020. The yellow box indicates the location of creepmeter XSH1. (c) Circles and squares (newly detected) show the latitudinal position of earthquakes, with gray bars showing the corresponding earthquake rate. The red line shows the fault surface slip recorded by creepmeter XSH1.

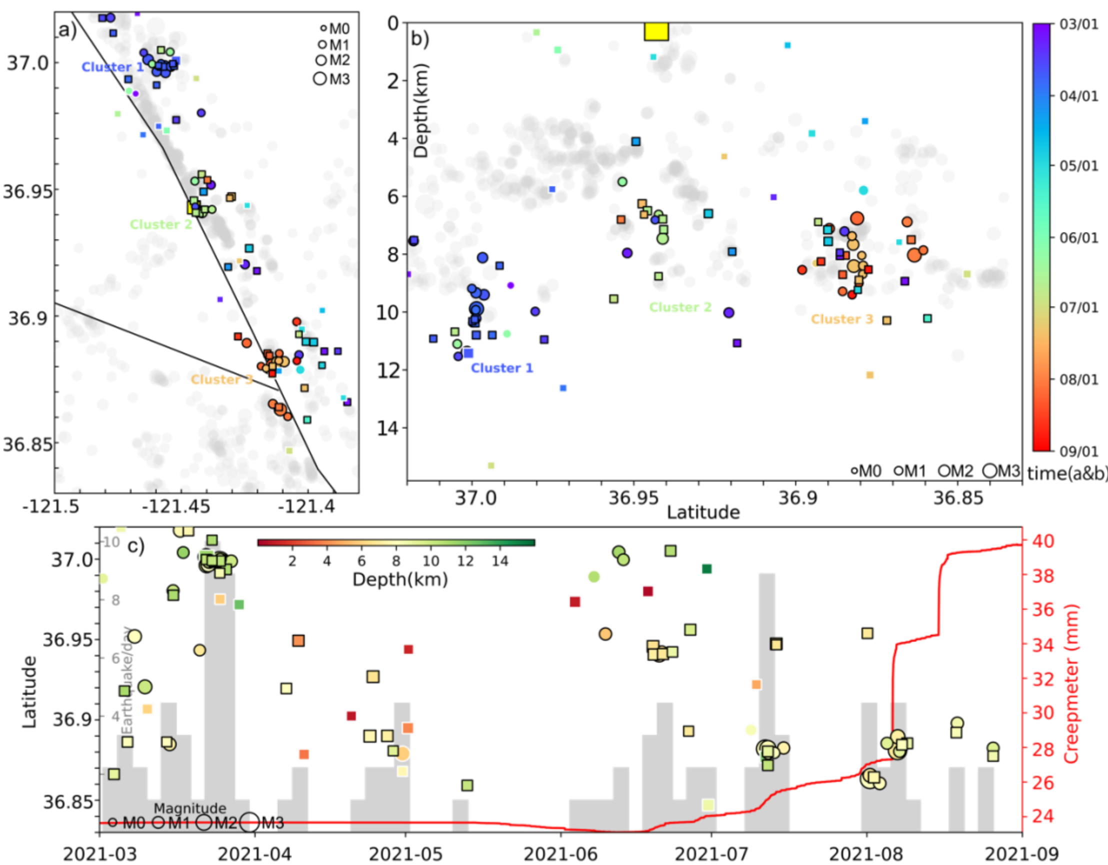

Figure S5. Normalized accumulated seismic moment along the fault in two distinct time periods, 2021-03-20 through 2021-05-20 (upper panel) and 2021-05-21 through 2021-09-01 (lower panel). Only events above magnitude completeness are plotted. Colored lines indicate moment accumulation from the starting date in the subtitle to the end date shown by the dots color. The sizes of dots are slightly different so that the lines would not fully block each other. Gray lines show the normalized accumulated seismic moment of earthquakes from 1984 to 2020. Gray bar marks the seismicity gap.

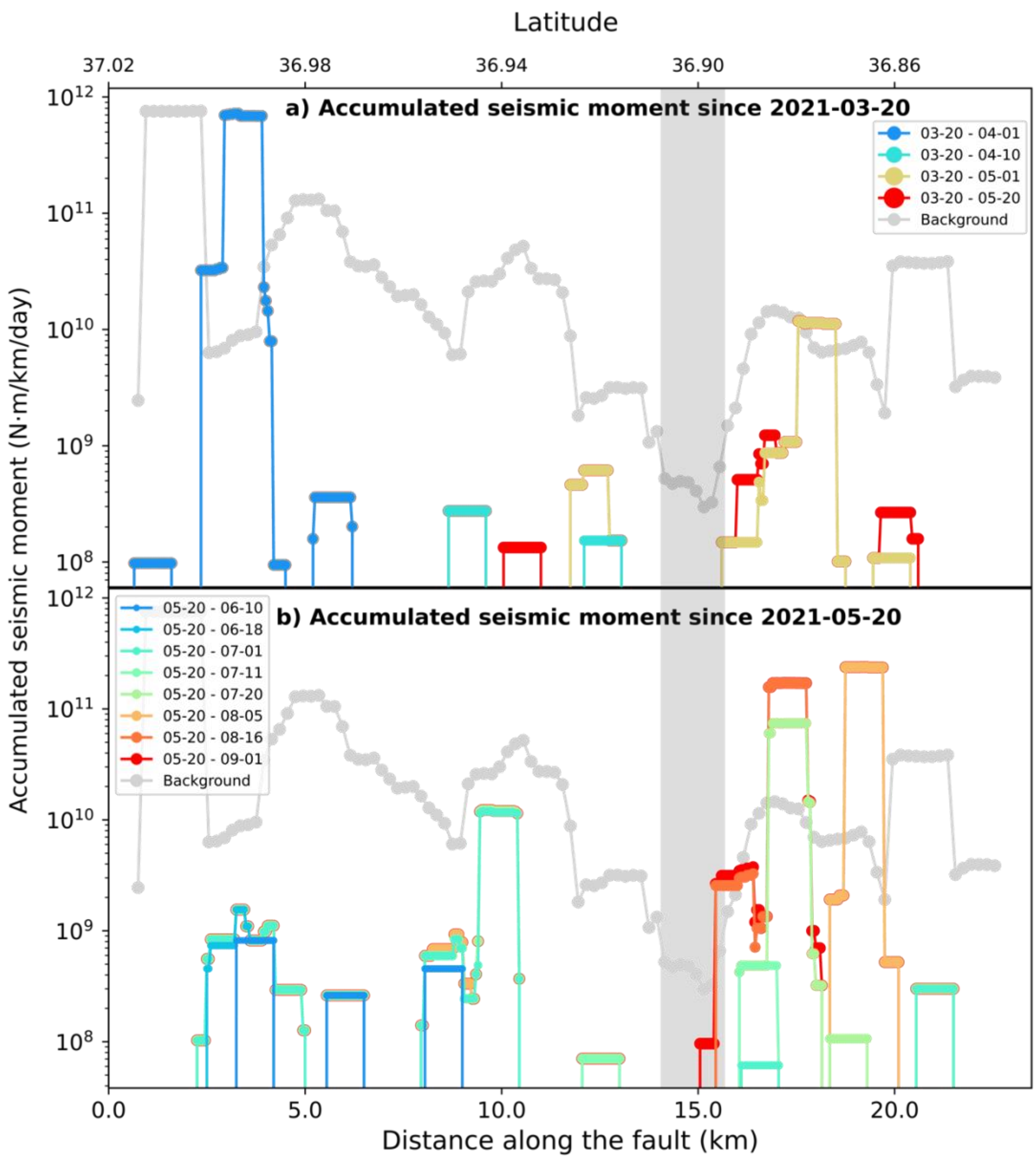

The misleading 'shallowing trend'

HYPOINVERSE allows the use of 1D velocity model or multiple velocity models. In a 1D velocity model, the seismic velocity varies only with depth and is constant within each depth layer. Multiple velocity models consist of many 1D velocity models for specific areas, accounting for regional variations. Transition regions between these models are managed using weighted averages of travel times and derivatives, ensuring transitions across different areas.

We tested the location of events in our 2021 catalog with the manually revised arrivals using the Coyote Lake 1-D velocity model (Table S3), and the results show a 'shallowing trend' from March to August (Figure S6a). Initially, it was misinterpreted as a migrating aseismic slip. However, upon extending our test to the location of all events in the NCEDC catalog from 2000 to 2022, the 'shallowing trend' still exists (Figure S6b). Comparing the location calculated with multiple velocity models (Figure S6c) against those obtained with a single velocity model for the 2000 to 2022 period, we concluded that the 'shallowing trend' is not indicative of an actual seismicity pattern but rather an artifact caused by the inherent limitations of the 1-D velocity model.

Table. S3. Coyote Lake 1D velocity model

Depth (km)	P-wave Velocity (km/s)
0.00	3.80
1.40	5.30
5.80	6.12
10.60	6.37
24.00	6.59
26.00	8.00

Fig.S6. Profile of earthquakes located by HYPOINVERSE with different velocity model and aperture. A) 2021 March-to-Sept. events from our catalog with revised arrival at selected stations using the Coyote Lake 1-D velocity model. B) 2000-2020 Events from the NCEDC catalog with NCEDC arrivals at all detecting stations using the Coyote Lake 1-D velocity model. C)2000-2020 Events from the NCEDC catalog with NCEDC arrivals at all detecting stations using multiple velocity models.

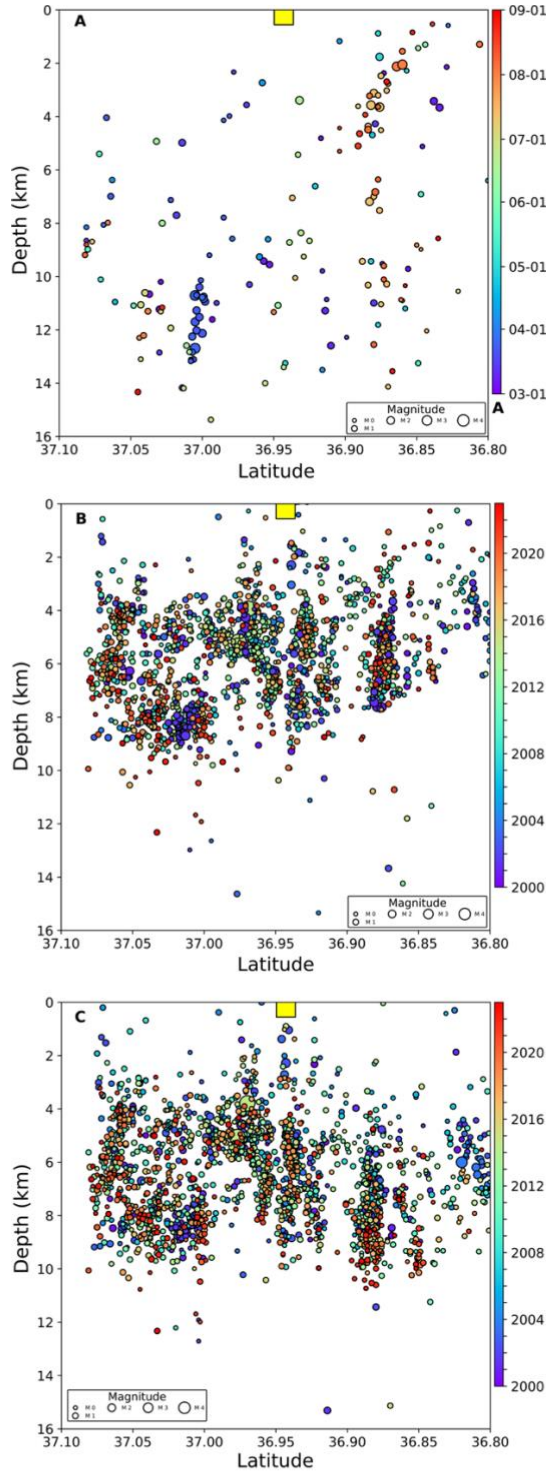
A
B
C
Depth (km)
Latitude
Magnitude
09-01
08-01
07-01
06-01
05-01
04-01
03-01
2020
2016
2012
2008
2004
2000
37.10
37.05
37.00
36.95
36.90
36.85
36.80

The along fault distances

The along-fault distances of the earthquakes are measured from the northwest point of the reference line in Figure S7 to the projections of the earthquakes on this line.

Figure S7. Along fault distances of earthquakes. The earthquakes are represented as dots color-coded by their distance along the fault. The reference line is plotted as the red dashed line.

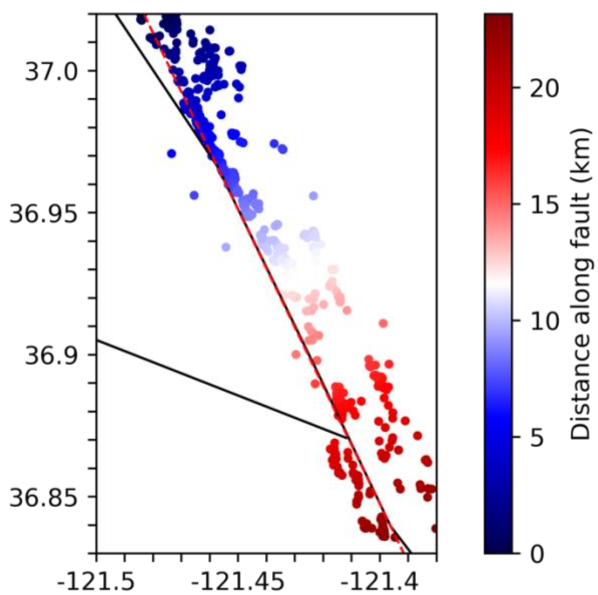

Normalized accumulated seismic moment

To address concerns regarding the comparison between the long-term accumulated seismic moment (1984-2020) and shorter time windows, we compared the accumulated seismic moment from 1984-2020 for all events and those smaller than M4.0. The comparison revealed a similar distribution, indicating that large events with longer recurrence intervals do not dominate the area.

Figure S8. Normalized accumulated seismic moment along the fault of historical earthquakes from 1984 to 2020.

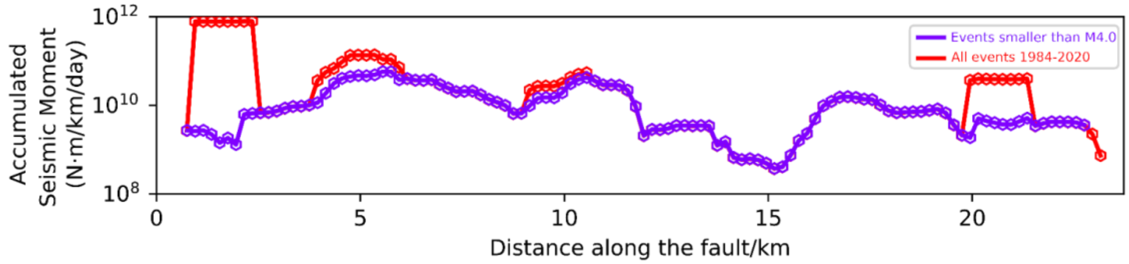
Accumulated
Seismic Moment
(N·m/km/day)
10^{12}
10^{10}
10^{8}
0
5
10
15
20
Distance along the fault/km
Events smaller than M4.0
All events 1984-2020